Int. J. Electrochem. Sci., 7 **(2012)** 12456 - 12469

International Journal of
ELECTROCHEMICAL
SCIENCE
www.electrochemsci.org

Corrosion Inhibition of Steel in Hydrochloric Acid Solution Using a Triazole Derivative: Electrochemical and Computational Studies

Yahia H. Ahmad, Walid M. I. Hassan[*]

Chemistry Department, Faculty of Science, Cairo University, Giza-12613, Egypt
[*]E-mail: walid_m76@yahoo.com

Received: 10 October 2012 / *Accepted:* 6 November 2012 / *Published:* 1 December 2012

The efficiency of 5,5'-[butane-1,4-diylbis(sulfanediyl)bis(4-amino-4H-1,2,4-triazole-3-thiol)] (BATT) as a corrosion inhibitor for mild steel in 2 M HCl was studied using polarization and electrochemical impedance spectroscopy (EIS). The adsorption of the investigated inhibitor onto the steel surface was found to follow Langmuir isotherm. The negative value of the free energy of adsorption, ΔG_{ads} ensures the spontaneity of the adsorption process. The temperature effect on the corrosion of steel in 2 M HCl with and without inhibitor was also studied. Moreover, density functional theory (DFT) calculations give a clear indication of strong molecular interaction between inhibitor molecules and iron surface.

Keywords: mild steel; triazole; polarization; EIS; acid inhibition; DFT.

1. INTRODUCTION

Stainless steel has a wide scope of applications in different industries which resulted in extensive research into its corrosion resistance in various aggressive environments. Acid solutions are widely used in industry as acid cleaning, acid descaling, acid pickling and oil well acidising. In these acid solutions inhibitors are required in order to protect metals and alloys from corrosion. Most of well-known acid inhibitors are heterocyclic compounds containing π-bonds, heteroatom phosphorous, sulfur, oxygen and nitrogen [1] as well as aromatic rings in their structure. The compounds that contain both nitrogen and sulfur can provide excellent inhibition, compared with compounds containing only nitrogen or sulfur [2,3]. Among various compounds that have been studied thiadiazole derivatives [4-6], triazole derivatives [7] and triazole thiol derivatives [8]. Although various experimental and theoretical techniques have been developed to study the structural properties of inhibitor molecules but

not many investigations were concerned with the interactions that occurred between the adsorbed molecules and metal surfaces.

The aim of this study is to investigate the corrosion of mild steel in 2 M HCl solution in the presence of a triazole derivative namely 5,5'-[butane-1,4-diylbis(sulfanediyl)bis(4-amino-4H-1,2,4-triazole-3-thiol)] (BATT) (see Fig. 1) and to simulate the interaction of its molecules on iron surface to get information about the mode and energy of this interaction.

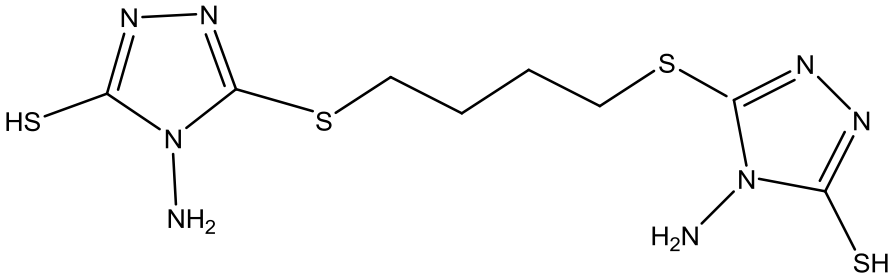

5,5'-(butane-1,4-diylbis(sulfanediyl))bis(4-amino-4*H*-1,2,4-triazole-3-thiol)

(**BATT**)

Figure 1. The molecular Structure of BATT

2. EXPERIMENTAL

Steel rod with the following chemical composition (wt%) C: 0.31; Si: 0.21; Mn: 0.81; P: 0.014; S: 0.017; Cu: 0.06; Cr: 0.02; Mo: 0.01; Ni: 0.02; V: 0.002 and balance Fe was fixed in a glass tube using epoxy resin leaving a constant surface area of 0.5 cm^2 to contact solution. A pre-treatment was carried out prior to each experiment, in which specimen surface was abraded with successive grades of emery papers up to 1200 grade, rinsed with bi distilled water, degreased in ethanol before immersion in test solution. The electrolytic solutions were prepared from analytical grade chemical reagent using bi distilled water. The solutions were used as naturally aerated and unstirred at 293K, unless stated otherwise. The molecular structure of the inhibitor is given in Scheme 1. The electrochemical measurements were carried out using a conventional three-electrode cell. A platinum sheet was used as auxiliary electrode and the reference electrode was Ag/AgCl electrode in saturated KCl solution. Polarization measurements were carried out at a scan rate of 1 mV s^{-1} using EG&G (Princeton Applied Research) model 273A Potentiostat/Galvanostat interfaced to an IBM PS/3 computer. Electrochemical impedance spectroscopy (EIS) measurements were carried out using the electrochemical workstation IM6e Zahner-electrik (GmbH, Meβtechnik, Kronach, Germany). The input signal was usually 10 mV peak to peak in the frequency domain 0.1-10^5 Hz. Before impedance or polarization measurements, the steel electrode was immersed in the test solution until a steady-state of the open circuit potential was reached. For surface examination, the scanning electron microscopy (SEM) photographs were taken with FEI Quanta 250 FEG instrument.

2.1. Computational details

The geometry optimization of the inhibitor and the electrode unit cell were performed using Gaussian 09W [9] at the DFT level of theory, using 6-31++G(d,p) basis set. The DFT calculations were carried out with the hybrid three-parameter density functional method abbreviated as B3LYP, which includes Beck's 3-parameter gradient exchange correction function (B3) [10] and the Lee, Yang and Parr correlation functional [11,12]. The geometry of the adsorbed inhibitor on the electrode was initially guessed by semi-empirical calculation using the PM6 Hamiltonian method [13] using quadratic convergent self-consistent Field (SCF) procedure [14]. This method is slower than regular SCF with Pulay's direct inversion in the iterative subspace (DIIS) extrapolation method [15] but is more reliable. The energy of interaction E_{int} was calculated by a full geometry optimization using B3LYP/LANL2DZ. The LANL2DZ basis set uses Los Alamos effective core potential (ECP) for core electrons plus DZ [16-18], which have a lesser effect on chemical bond formation. By use of this basis set, computational time and convergence difficulties are considerably reduced. The calculated E_{int} were corrected using basis set superposition error (BSSE) correction [19,20].

3. RESULTS AND DISCUSSION

3.1. Potentiodynamic polarization measurements

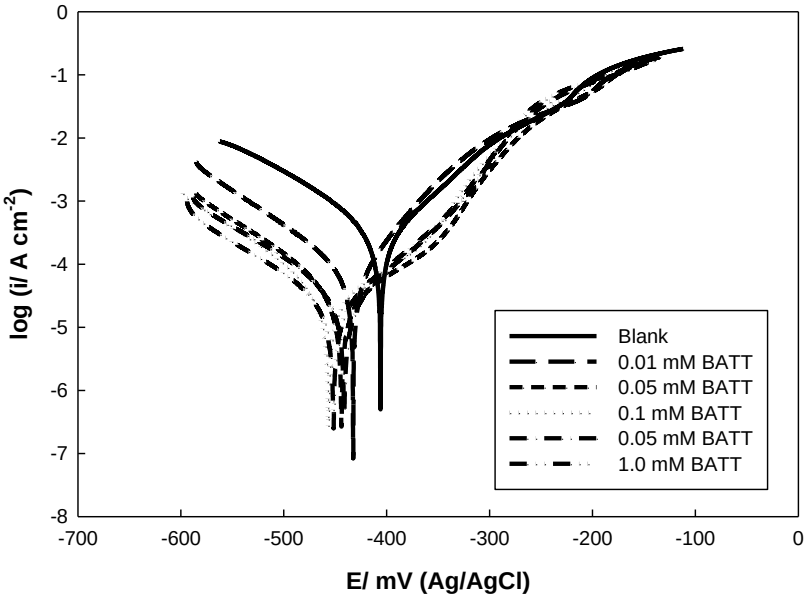

Figure 2. Potentiodynamic polarization curves for mild steel in 2 M HCl in absence and presence of different concentrations of BATT.

Figure 2 represents Tafel polarization curves of mild steel in 2 M HCl in the presence and absence of various concentrations of the inhibitor BATT at 293K. It can be observed that both anodic

and cathodic currents were reduced in the presence of BATT, but the reduction is more pronounced in the cathodic current than anodic current which means that the addition of inhibitor molecules reduces the anodic dissolution and also retards the hydrogen evolution (the main cathodic reaction in acidic medium).

In acidic medium the reduction of H^+ ions at mild steel surface takes place through a charge transfer mechanism [6]. The inhibitor molecules are first adsorbed onto the mild steel surface and, therefore, blocking the active sites of the surface. In this way, the surface area available for H^+ ions is decreased whereas the reaction mechanism is not affected [21].

The electrochemical kinetic parameters, i.e. corrosion potential (E_{corr}), cathodic and anodic Tafel slopes (β_c and β_a) and corrosion current density (i_{corr}), obtained by extrapolation the Tafel lines, are presented In Table 1. The inhibition efficiency ($\eta\%$) was calculated according to the relation [22]:

$$\eta\% = \frac{i^0_{corr} - i_{corr}}{i^o_{corr}} x100 \quad (1)$$

Where i^0_{corr} and i_{corr} are the corrosion current densities in the absence and presence of inhibitor, respectively. Data represented in Table 1 also reveals that the inhibition efficiency, ($\eta\%$) increases with increasing the inhibitor concentration indicating a higher coverage of inhibitor at higher concentrations of inhibitor.

Table 1. Polarization parameters for mild steel in 2 M HCl in absence and presence of different concentrations of BATT at 293K

Inhibitor concentration / mmol L^{-1}	E_{Corr} / mV (Ag/AgCl)	i_{Corr} / μA cm^{-2}	β_a / mV $decade^{-1}$	β_c / mV $decade^{-1}$	Inhibition efficiency η_p/ %
-	-406.0	379.9	98.99	131.8	-
0.01	-433.3	43.91	122.7	88.18	88.44
0.05	-440.8	21.65	65.71	91.71	94.30
0.10	-443.0	17.62	66.21	95.53	95.36
0.50	-458.3	14.62	53.46	97.32	96.15
1.00	-451.8	7.48	60.30	79.14	98.03

The cathodic polarization curves give rise to parallel Tafel lines with close values of cathodic Tafel slopes (β_c) indicating that the addition of inhibitor to the aggressive solution does not modify the proton reduction mechanism and this reaction is activation-controlled. The inhibitor is adsorbed on the metal surface blocking the active sites available for H^+ ions reduction but the actual reaction mechanism remains unaffected [23].

A compound can be classified as an anodic or a cathodic type inhibitor when the change in the corrosion potential, E_{corr} value is larger than 85 mV [24]. Since no such large displacement exhibited by BATT in the values of E_{corr} (Table 1), then this molecule can be considered as a mixed-type

inhibitor. The value of the corrosion potential, E_{corr} is shifted to more negative potentials on addition of increasing concentrations of BATT which proves that the inhibitor affects the cathodic reaction more than the anodic reaction. Accordingly, BATT can be considered as a mixed type (anodic/cathodic) inhibitor with a predominantly cathodic reaction.

3.2. EIS measurements

EIS provides a rapid and convenient way to evaluate the performance of the organic-coated metals and has been widely used for investigation of protective properties of organic inhibitors on metals [25]. Figure 3 shows the Nyquist plots for mild steel in 2 M HCl solution in absence and presence of different concentrations of BATT at 20 °C. It is obvious that plots are in the form of semicircles which have diameters increases with increasing the concentration of the solution indicating adsorption of inhibitor molecules on the metal surface. The impedance spectra for the Nyquist plots were analyzed by fitting to the equivalent circuit model shown in Fig. 4.

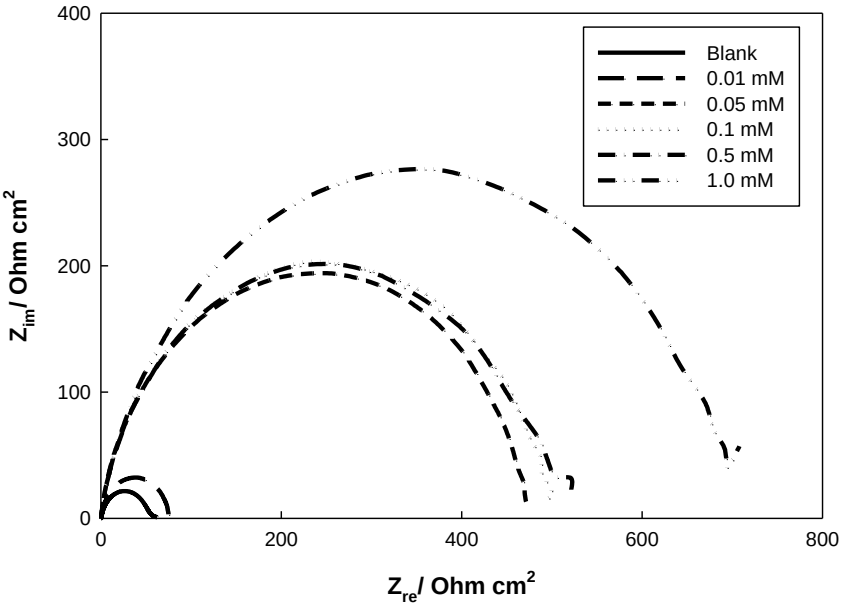

Figure 3. Nyquist impedance plots for mild steel in 2 M HCl in absence and presence of different concentrations of BATT.

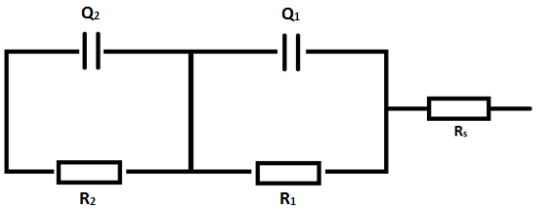

Figure 4. The equivalent circuit model used to fit the experimental impedance data.

The equivalent circuit model consists of two circuits in series, R_1Q_1 and R_2Q_2 parallel combination and the two are in series with R_s. In this model, R_s, represents the electrolyte resistance, Q_1 is capacitance of the double layer and R_1 is the charge transfer resistance, whereas, Q_2 and R_2 are the capacitance and resistance of the passive layer on the steel surface, respectively. The fitted values of resistances and capacitances are listed in Table 2. From the obtained data in the table it can be observed that the film resistance, R_2 increases with increasing the inhibitor concentration while the capacitance, Q_2 decreases, indicating the formation of a protective film on the metal surface whose thickness increases with the increase in inhibitor concentration [26].

Table 2. Impedance parameters for mild steel in 2 M HCl in absence and presence of different concentrations of BATT at 293K

Inhibitor Concentration/ mmol L^{-1}	R_S/ Ohm cm^2	R_1/ Ohm cm^2	Q_1/ μF cm^{-2}	α_1	R_2/ Ohm cm^2	Q_2/ μF cm^{-2}	α_2	η_I (%)
-	0.5090	15.1350	248.80	0.997	40.805	119.26	0.837	-
0.01	0.5060	29.3750	121.60	0.966	406.680	87.660	0.866	89.96
0.05	0.4515	33.8450	146.82	0.960	435.70	38.640	0.911	90.64
0.10	0.6410	32.1900	99.960	0.960	469.85	22.480	0.890	91.32
0.50	0.3550	26.5500	119.20	0.954	475.10	22.880	0.895	91.41
1.00	0.3545	26.1350	95.240	0.990	658.50	19.590	0.897	93.80

The percentage inhibition efficiencies of different concentrations of BATT were calculated using the following equation:

$$\eta\% = \frac{R_{2(inh)} - R_{2(uninh)}}{R_{2(inh)}} x100 \qquad (2)$$

Where $R_{2(uninh)}$ and $R_{2(inh)}$ are the film resistance in absence and presence of inhibitor, respectively. The percentage inhibition efficiencies and values of different components in the equivalent circuit model are given in Table 2. The data of Table show that addition of BATT into the acid media leads to increase in the value of R_{ct} and consequently the inhibition efficiency which may suggest the formation of a protective layer of increasing thickness on the metal surface [27].

3.3 Adsorption isotherm

Corrosion inhibition occurs via adsorption of the organic molecule on the corroding metal surface, following some known adsorption isotherms, with the polar groups acting as the reactive centers in the molecules. The resulting adsorption film acts as a barrier that isolates the metal from the

corroding environment and the efficiency of inhibition depends on the mechanical, structural and chemical characteristics of the adsorption layers formed under particular conditions.

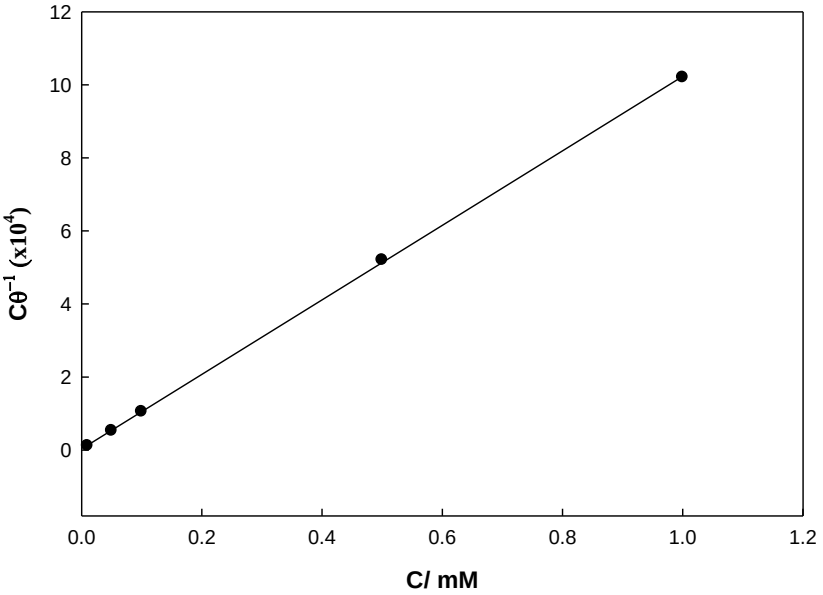

Figure 5. Langmuir adsorption isotherm plot of BATT on mild steel in 2 M HCl at 293K.

The adsorption isotherms describe the molecular interaction between the inhibitor molecules and the active sites on the metal surface [28]. Several adsorption isotherms were tested in order to find the best suitable adsorption isotherm describing the adsorption of BATT onto mild steel in 2 M HCl where Langmuir adsorption isotherm was found the most suitable one. Langmuir adsorption isotherm can be expressed by the following equation [29]:

$$\frac{C_{inh}}{\theta} = \frac{1}{K_{ads}} + C_{inh} \quad (3)$$

Where θ is the degree of coverage on the metal surface, C_{inh} is the inhibitor concentration in the electrolyte and K_{ads} is the equilibrium constant for the adsorption/desorption process. A representative Langmuir adsorption isotherm using potentiodynamic polarization data is given in Fig. 5.

The value of equilibrium constant, K_{ads} calculated from the reciprocal of the intercept of the isotherm line was found to be 833.3 L mol^{-1}. The standard free energy of adsorption, ΔG_{ads} can be evaluated according to the relation:

$$\Delta G^{0}_{ads} = -RT\ln(55.5K_{ads}) \quad (4)$$

The standard free energy of adsorption values of –20 kJ mol^{-1} or less negative values are exhibited when an electrostatic interaction between charged molecules and charged metal surface (physical adsorption), whereas values of –40 kJ mol^{-1} or more negative involves charge sharing or

transfer from the inhibitor molecules to the metal surface to form a coordinate covalent bond [30]. The calculated standard free energy of adsorption for BATT was found -16.38 kJ mol^{-1}, which ensures that adsorption is spontaneous and adsorption type is physical [28,31].

3.4 Effect of temperature

The activation energy of corrosion process can be obtained by investigating the influence of temperature on the corrosion and corrosion inhibition. Consequently some information about adsorption mechanism of the inhibitor can be obtained from the activation energy values. A plot of ln i_{corr} vs T^{-1} obeys Arrhenius equation [32]:

$$\ln i_{corr} = -\frac{E_a}{RT} + \text{constant} \quad (5)$$

The potentiodynamic polarization measurements were performed at different temperatures (from 293K to 323K) in the absence and presence of BATT. It was found that the corrosion current density increases with the increase in temperature both in uninhibited and inhibited solutions (Fig. 6). The activation energy was calculated from the slope of the linear relation and found to be 57.13 and 54.77 kJ mol^{-1} in absence and presence of BATT, respectively. The lower value of activation energy in the presence of inhibitor may be attributed to the chemisorptions of the inhibitor [33] which is not our case. Other explanation is that the inhibitor is adsorbed on the most active adsorption sites (having lower energy) and the corrosion process takes place predominantly on the less active sites of higher energy resulting in increase of activation energy than in uninhibited solutions [34].

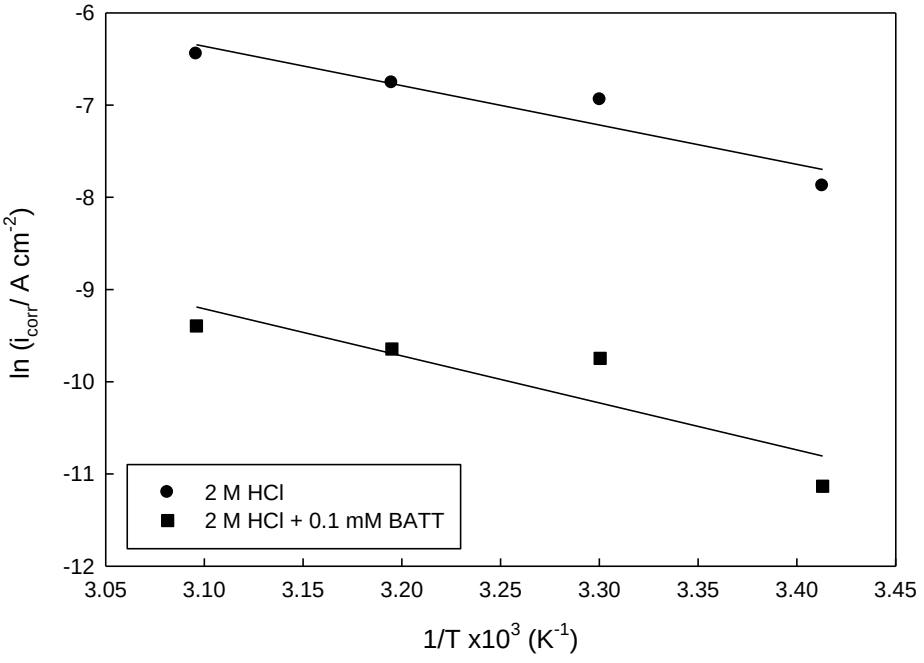

Figure 6. Arrhenius plots for mild steel in 2 M HCl in absence and presence of 0.1 mM BATT.

3.5. Quantum chemical calculations

The optimized geometry of BATT is shown in Fig. 7. The positions of atoms were carefully checked by testing all possible free rotations to achieve a global minimum which is further confirmed by a frequency calculation. The structure has symmetrical bond lengths due to possessing C_i point group. The natural bond order atomic charges are shown in Fig. 7.

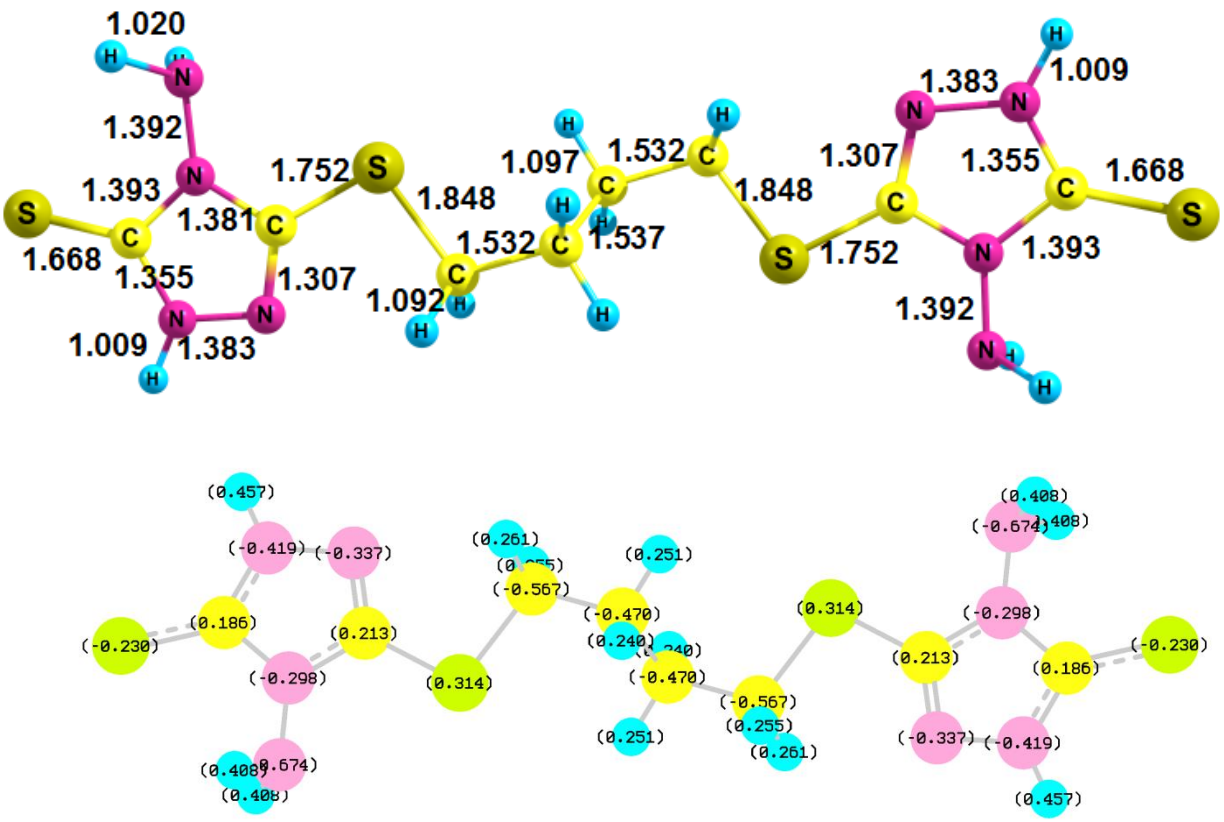

Figure7. The optimized geometry of BATT (bond lengths are in Å) and natural bond orbital atomic charges.

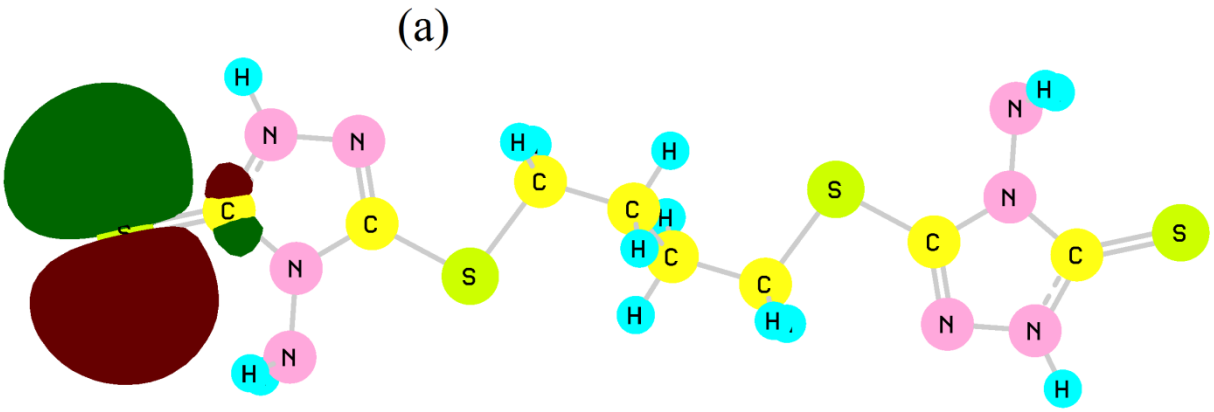

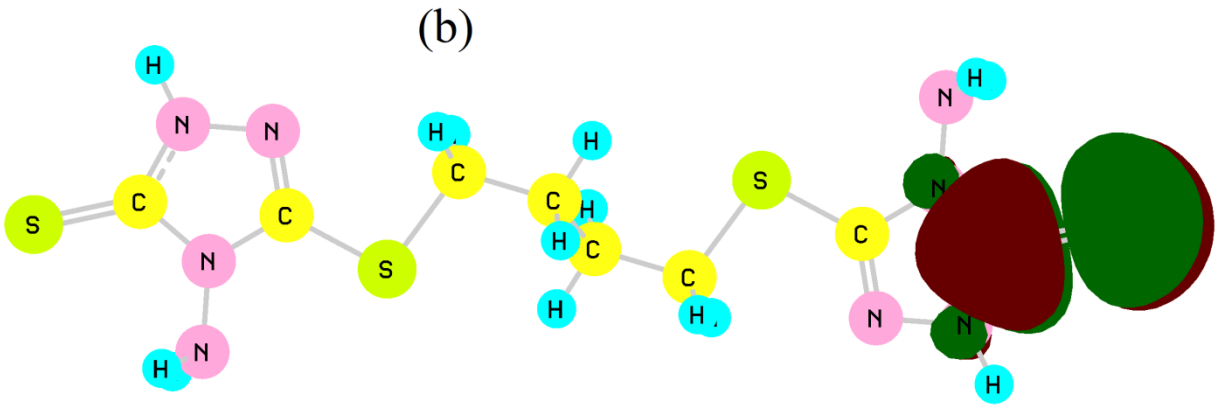

Figure 8.The molecular orbital plots of (a) HOMO and (b) LUMO.

The most negative atom is the nitrogen of the amino group (0.674) followed by the aliphatic carbons in CH_2 chain (-0.57 ~ 0.47). Atomic charges suggest a possibility of interaction between aliphatic carbons and steel. The molecular orbital plot of highest occupied molecular orbital (HOMO) and lowest unoccupied molecular orbital (LUMO) are shown in Fig. 8. HOMO is localized over one triazole ring while LUMO is localized on the other triazole ring this suggests that only one triazole ring is involved in the adsorption over steel.

Table 3. Total energy, energy of HOMO, LUMO, ΔE and interaction energy E_{int} in kCal/mol and dipole moment in debye.

	BATT	1,2,4-Triazole
Total E	-1470903.336	-152025.753
E_{HOMO}	-138.454	-178.658
E_{LUMO}	-16.378	-11.847
ΔE	122.076	166.811
μ, Debye	0.0025	2.945
E_{int}(BSSE)	85.05	32.14

The calculated parameters such as energy of HOMO, LUMO and dipole moment (μ) of BATT and 1,2,4-triazole are given in Table 3. The values are compared to 1,2,4-triazole since it is the base of our Inhibitor and it has a well known inhibition efficiency [35]. E_{HOMO} often indicates the electron donating ability of the molecule and so inhibition efficiency increases with E_{HOMO}. The energy gap (ΔE) between LUMO and HOMO is a parameter with the smaller value causes higher inhibition efficiencies of the molecule [36,37]. Both E_{HOMO} and ΔE indicates higher inhibition efficiency of BATT over 1,2,4-triazole. The dipole moment (μ) is almost zero because of symmetry. This explains the weaker solubility of the BATT in polar solvents.

The optimized unit cell of steel is a body centered cube which is shown in Fig. 9a. The distance between Fe atom in the center and Fe atoms at the corners is 2.085 Å and the edge distance is 2.408 Å.

Multiple of the unit cell were used to calculate the interaction energy. The optimized geometry of the adsorbed BATT on steel is shown in Fig. 9b. The triazole compounds studied here are organic bases which can be protonated in an acid medium, at the nitrogen atoms.

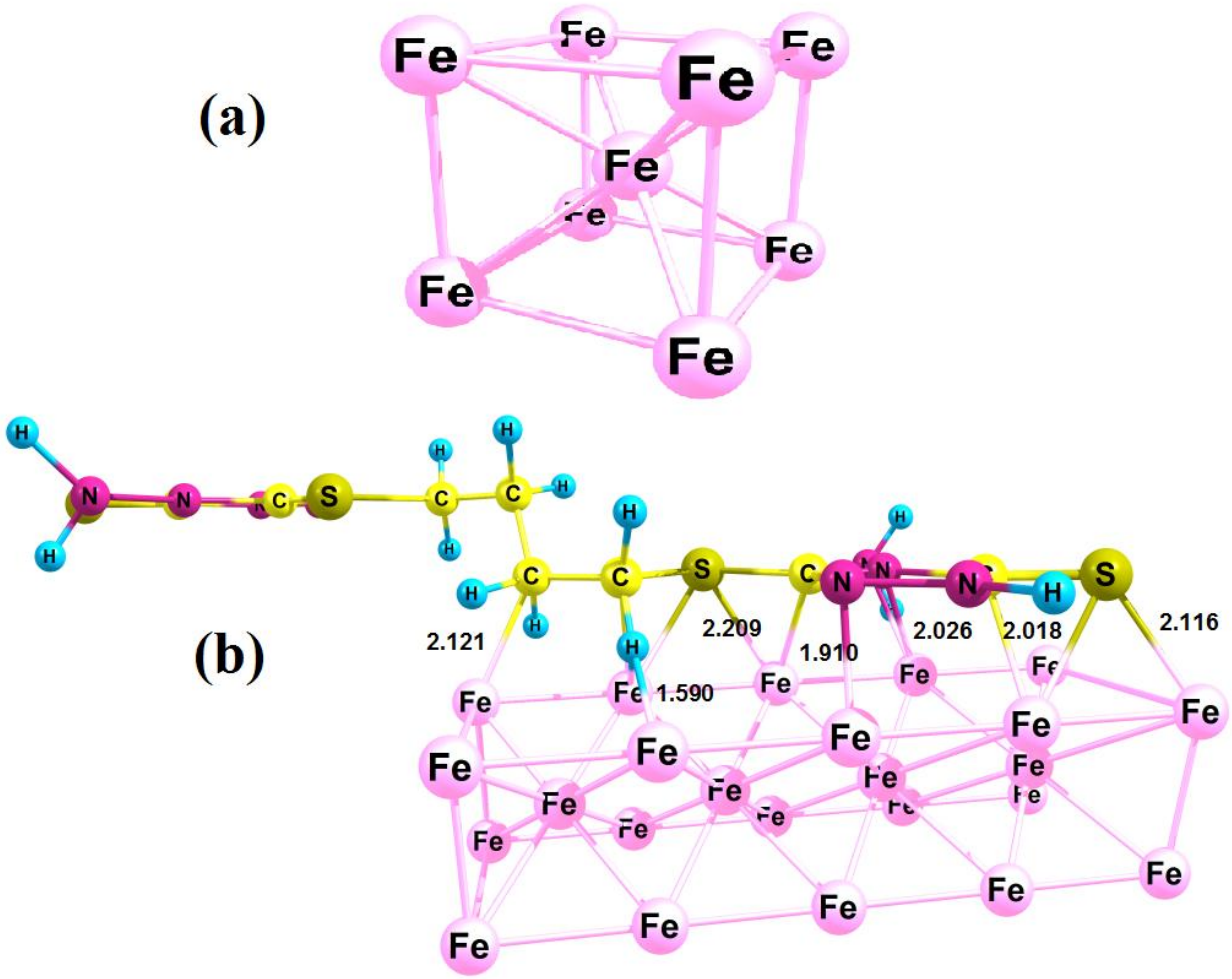

Figure 9. The optimized geometry of (a) steel unit cell and (b) adsorbed BATT on steel (bond lengths are in Å).

Thus, they become cations, the inhibitor cation adsorbs on the metal surface and releases protons. The overall process is shown in reaction (8).

$$Inhibitor\ molecule + H^{+} \longrightarrow Inhibitor\ cation \quad (6)$$

$$Inhibitor\ cation + Cluster \longrightarrow Inhibitor - cluster + H^{+} \quad (7)$$

$$Inhibitor\ molecule + Cluster \longrightarrow Inhibitor - cluster \quad (8)$$

Therefore, the interaction energy between the inhibitor molecule and the metal surface, E_{int}, is the sum of the energies of steps (6) and (7) and can be calculated according to Eq. (9):

$$E_{\text{int}} = E_{inhibitor-cluster} - (E_{inhibitor} + E_{cluster}) \quad (9)$$

Where, $E_{inhibitor-cluster}$, $E_{inhibitor}$ and $E_{cluster}$ are electronic energies of the inhibitor–mild steel system, the inhibitor compound and the mild steel cluster, respectively. The values of E_{int} and the binding energy ($E_{binding}$ = - $E_{interaction}$) are shown in Table 3. The high value of E_{int} suggests that adsorption via many centers. Fig. 9b shows that many sites of interaction exist between BATT and steel mainly on the triazole ring and some weaker interactions occur between the sulfur and steel as well as aliphatic CH_2 and steel.

3.6 Scanning electron microscopy

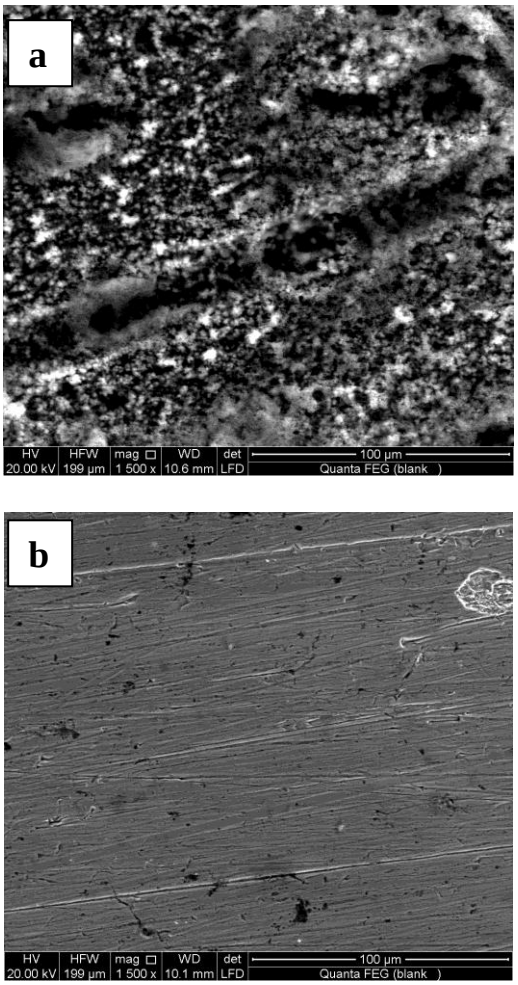

Figure 10. SEM images of mild steel surface after 2h immersion in (a) 2 M HCl (b) 2 M HCl containing 0.1 mM BATT at 293K.

Scanning electron microscopy photographs obtained for mild steel surface after immersion in 2 M HCl solution for 120 min in the absence and presence of 0.1 mM BATT are shown in Fig. 10. The steel surface was greatly corroded in HCl solution in absence of BATT (Fig. 10a). On the other hand, it can be observed that the addition of BATT results in formation of a protective layer on the surface which greatly reduces the corrosion rate (Fig. 10b).

4. CONCLUSIONS

- The studied triazole derivative BATT greatly inhibits the corrosion of steel in 2.0 M HCl and the inhibition efficiency increases with increasing the inhibitor concentration.
- The results of potentiodynamic polarization reveal that the used inhibitor affects the cathodic reaction more than the anodic but still a mixed type inhibitor.
- The adsorption of BATT on steel surface obeys Langmuir isotherm and its mode is physical adsorption.
- DFT calculations reveal that BATT has many sites of interaction with steel which explains its high energy of interaction. Energetic explains the higher inhibition efficiency of BATT over 1,2,4-triazole.

References

1. S. A. Abd El-Maksoud, *Appl. Surf. Sci*. 206 (2003) 129.
2. J. Aljourani, M. A. Golozar, K. Raeissi, *Mater. Chem. Phys*. 121 (2010) 320.
3. Y. Abboud, A. Abourriche, T. Saffaj, M. Berrada, M. Charrouf, A. Bennamara, N. Al Himidi, H. Hannache, *Mater. Chem. Phys*. 105 (2007) 1.
4. J. M. Bastidas, E. Otero, *Mater. Corros*. 47 (1996) 333.
5. E. Otero, J. M. Bastidas, *Mater. Corros*. 47 (1996) 133.
6. Y. Tang, X. Yang, W. Yang, R. Wan, Y. Chen, X. Yin, *Corros. Sci*. 52 (2010) 1801.
7. K. F. Khaled, *Electrochim. Acta* 53 (2008) 3484.
8. A. Y. Musa, A. A. H. Kadhum, M. S. Takriff, A. R. Daud, S. K. Kamarudin, A. Muhamad, *Corros. Eng. Sci. Tech.* 45 (2010) 163.
9. M. J. Frisch, G. W. Trucks, H. B. Schlegel, G. E. Scuseria, M. A. Robb, J. R. Cheeseman, G. Scalmani, V. Barone, B. Mennucci, G. A. Petersson, H. Nakatsuji, M. Caricato, X. Li, H.P. Hratchian, A. F. Izmaylov, J. Bloino, G. Zheng, J.L. Sonnenberg, M. Hada, M. Ehara, K. Toyota, R. Fukuda, J. Hasegawa, M. Ishida, T. Nakajima, Y. Honda, O. Kitao, H. Nakai, T. Vreven, J. A. Montgomery Jr., J. E. Peralta, F. Ogliaro, M. Bearpark, J. J. Heyd, E. Brothers, K. N. Kudin, V. N. Staroverov, R. Kobayashi, J. Normand, K. Raghavachari, A. Rendell, J. C. Burant, S.S. Iyengar, J. Tomasi, M. Cossi, N. Rega, N. J. Millam, M. Klene, J. E. Knox, J.B. Cross, V. Bakken, C. Adamo, J. Jaramillo, R. Gomperts, R. E. Stratmann, O. Yazyev, A. J. Austin, R. Cammi, C. Pomelli, J. W. Ochterski, R. L. Martin, K. Morokuma, V. G. Zakrzewski, G. A. Voth, P. Salvador, J. J. Dannenberg, S. Dapprich, A. D. Daniels, Ö. Farkas, J. B. Foresman, J. V. Ortiz, J. Cioslowski, D. J. Fox, GAUSSIAN 09, Revision A1, Gaussian, Inc, Wallingford, CT, 2009.
10. A. D. Becke *J. Chem. Phys*. 98 (1993) 5648.
11. C. Lee, W. Yang, R. G. Parr, *Phys. Rev.* B 37 (1988) 785.
12. B. Miehlich, A. Savin, H. Stoll, H. Preuss, *Chem. Phys. Lett*. 157 (1989) 200.
13. J. J. P. Stewart, *J. Mol. Model*. 13 (2007) 1173.

14. G. B. Bacskay, *Chem. Phys*. 61 (1981) 385.
15. P. Pulay, *J. Comp. Chem*. 3 (1982) 556.
16. P. J. Hay and W. R. Wadt, *J. Chem. Phys*. 82 (1985) 270.
17. W. R. Wadt and P. J. Hay, *J. Chem. Phys*. 82 (1985) 284.
18. P. J. Hay and W. R. Wadt, *J. Chem. Phys*. 82 (1985) 299.
19. S. F. Boys, F. Bernardi, *Mol. Phys*. 19 (1970) 553.
20. S. Simon, M. Duran, and J. J. Dannenberg, *J. Chem. Phys*. 105 (1996) 11024.
21. R. Solmaz, G. Kardas, B. Yazici, M. Erbil, *Coll. Surf. A. Physicochem. Eng. Aspects* 312 (2008) 7.
22. B. El Mehdi, B. Mernari, M. Traisnel, F. Bentiss, M. Lagrenée, *Mater. Chem. Phys*. 77 (2002) 489.
23. R. Fuchs-Godec, *Coll. Surf. A. Physicochem. Eng. Aspects* 280 (2006) 130.
24. H. Ashassi-Sorkhabi, M. R. Majidi and K. Seyyedi, *Appl. Surf. Sci*. 225 (2004) 176.
25. R. Solmaz, G. Kardas, M. Culha, B. Yazici, M. Erbil, *Electrochim. Acta* 53 (2008) 5941.
26. S. K. Shukla, M. A. Quraish, *Mater. Chem. Phys*. 120 (2010) 142.
27. J. R. Macdonald, W. R. Kenan, in: J. R. Macdonald (Ed.), Impedance Spectroscopy: Emphasizing Solid Materials and Systems, Wiley, New York, 1987, P. 39.
28. K. C. Emregul, E. Duzgun, O. Atakol, *Corros. Sci*. 48 (2006) 3243.
29. N. Caliskan, E. Akbas, *Mater. Chem. Phys*. 126 (2011) 983.
30. S. V. Ramesh, A. V. Adhikari, *Mater. Chem. Phys*. 115 (2009) 618.
31. H. Ashassi-Sorkhabi, B. Shaabani, D. Seifzadeha, *Electrochim. Acta* 50 (2005) 3446.
32. P. W. Atkin, Physical Chemistry, 5th ed., University Press, Oxford, 1994, P. 877.
33. A. Popova, E. Sokolova, S. Raicheva, M. Christov, *Corros. Sci*. 45 (2003) 33.
34. Y. Tang, X. Yang, W. Yang, Y. Chen, R. Wan, *Corros. Sci*. 52 (2010) 242.
35. K. F. Khaled, *Electrochim. Acta* 53 (2008) 3484.
36. S. M. A. Hosseini, A. Azimi, *Corros. Sci.* 51 (2009) 728.
37. M. Mousavi, M. Mohammadalizadeh, A. Khosravan, *Corros. Sci*. 53 (2011) 3086.